Self-Assembly of α-Tocopherol Transfer Protein Nanoparticles – a Patchy-Protein Model

Raphael Peltzer,[†] Hima Bindu Kolli,[†] Achim Stocker,[*,‡] and Michele Cascella[*,†]

[†]*Department of Chemistry, and Hylleraas Centre for Quantum Molecular Sciences, University of Oslo, PO Box 1033 Blindern, 0315 Oslo, Norway*

[‡]*Deparment of Chemistry and Biochemistry, University of Bern, Freiestrasse 3, 3012 Bern, Switzerland*

E-mail: achim.stocker@dcb.unibe.ch; michele.cascella@kjemi.uio.no

Abstract

We describe the mechanism of self-aggregation of α-tocopherol transfer protein into a spherical nano-cage employing by Monte Carlo simulations. The protein is modelled by a patchy coarse-grained representation, where the protein-protein interfaces, determined in the past by x-ray diffraction, are represented by simplified two-body interaction potentials. Our results show that the oligomerization kinetics proceeds in two steps, with the formation of meta-stable trimeric units, and the subsequent assembly into the spherical aggregates. Data are in agreement with experimental observations regarding the prevalence of different aggregation states at specific ambient conditions. Finally, our results indicate a route for the experimental stabilization of the trimer, crucial for the understanding of the physiological role of such aggregates in vitamin E body trafficking.

Introduction

α-tocopherol transfer protein (α-TTP hereafter) it the liver factor responsible for the retention of RRR-α-tocopherol (α-tol), the active isoform of vitamin E, in the human body.[1–3] α-TTP solubilizes α-tol from the external leaflet of maturing endosomal compartments, promoting its release into the blood. Structural studies over the years[4,5] indicate that α-TTP is active as a monomer, similarly to other transporters of its family.[6–8] Unlike for retention, the mechanism(s) by which α-tol is secreted into the blood, and then absorbed into the target tissues, is at present not well understood. Possible pathways for the secretion and blood transport of α-tol include enrichment into the leaflets of the plasma membrane by a lipid-exchange mechanism,[9,10] and transport into the blood by aggregating to very-low density lipoprotein vesicles.[2] The absorption from the blood into the target tissues is even less understood, but it must imply some mechanism of recognition in order to bypass endothelial barriers, like the blood-brain barrier or the placenta.

The involvement of α-TTP into α-tol trafficking has not been clearly defined. In a recent work, Arai and coworkers have suggested that transfer of α-tol to the plasma membrane is coupled to the extraction of phosphatidylinositolphosphates (PIPs) from the same membrane by α-TTP.[3] Interestingly, they also suggested that lipid-exchange at the plasma membrane may involve higher order aggregates of α-TTP than the monomers.[3]

Very recently, we provided structural evidence that upon binding to α-tol, α-TTP acquires the tendency to oligomerize.[11] The oligomerised proteins form stable, regular spherical nanoparticles composed of 24 α-TTP units (α-TTP$_S$), which could be characterized by a series of methods, including cryo-EM and X-ray diffraction (PDB: 5MUE and 5MUG).[11] Thermal analysis demonstrated that α-TTP$_S$ is thermodynamically stable; furthermore, oxidative conditions enhance its stability by promoting the formation of twelve disulfide-bonds cross-linking different α-TTP units. The X-ray crystallography data of α-TTP$_S$ revealed a regular assembly of 24 monomers organized in a cubic symmetry. Each α-TTP unit is located on one vertex of a cantellated cube, and it is involved in two kinds of molecular contacts with four neighboring proteins (Figure 1). The first interface builds around the C_4 symmetry axis of the assembly, and it is constituted by a patch of

surface amino acids that are exposed to the solvent in the native monomeric folding of α-TTP . The second interface is responsible for the assembly of α-TTP around the trimeric C_3 axis. This interface is located on the surface of the proper SEC-14-like binding domain; in α-TTP it is screened from the solvent by the N-terminal helical domain. In α-TTP$_S$, the interfaces are accessible to the partner proteins thanks to the unfolding of the first N-terminal helix, which is not detectable in the corresponding X-ray structure. The partial unfolding of the N-terminal helix is triggered by external conditions, including binding to α-tol or interaction with negatively-charged lipids.[11]

α-TTP$_S$ shows selective and efficient transport properties through *in vitro* models of endothelial barriers,[11] making it a potential candidate as one of the physiological route for the delivery of vitamin E into the brain.[12,13] As much as oligomerization of α-TTP is crucial for its transfecting properties, its mechanistic aspects remain obscure. In particular, chromatographic data showed that when the monomeric form is the most stable aggregation state for α-TTP , this is at equilibrium with a small presence of low-weight dimeric or tetrameric aggregates. On the contrary, when the aggregation into the high weight is triggered, the only species present in the solution are monomeric α-TTP or regular α-TTP$_S$ constructs, while no other low-, middle-weight assemblies coexist at detectable concentration.[11]

In the present study, we investigated the formation of α-TTP$_S$ using Monte Carlo simulations of a toy patchy-model of α-TTP. Molecular simulations using patchy models are proven to be very effective in understanding the nature of self assembly in systems like patchy colloids, soft functionalized nanoparticles and biomolecules.[14–17] In particular, models with anisotropic and highly directional interacting patches are particularly suited to describe protein assembly.[18–23]

Computational Methods

Computational model The patchy model for one α-TTP consisted of one hard sphere, with four interaction sites (IS) located on its surface (Figure 1). The relative orientation of the IS was chosen to mimic the geometric organization of α-TTP$_S$. Interactions were imposed between IS$_{\mathrm{A}}$ and IS$_{\mathrm{B}}$,

and between IS_C and IS_D types, consistently with the experimental structure of α-TTP_S.

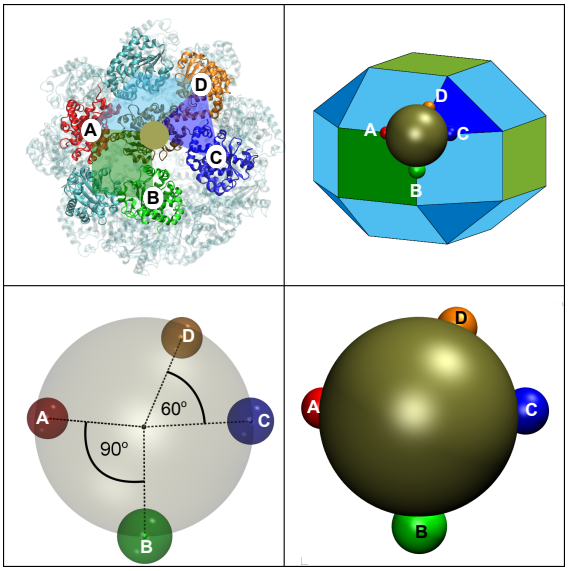

Figure 1: Coarse Grained model of α-TTP_S. *Top:* (left) In the native α-TTP_S, any monomeric α-TTP (gold spot) is in contact with four other proteins along the edges of a cantellated cube (top right). *Bottom:* α-TTP is described as a sphere with four interaction sites corresponding to the protein-protein contacts in α-TTP_S.

The interaction potentials for the two IS pairs were described by toy potential wells of depth $E_{A/B} = u$, $E_{C/D} = 3u$ (u being an arbitrary unit of energy), dependent on both the distance between the IS, and the relative orientation of the proteins. The initial 1:3 ratio between $E_{A/B}$ and $E_{C/D}$ was calibrated on an estimate of the dimerization free-energies from atomistic models using a standard thermodynamic cycle,[24] computing the solvation free energy of individual and dimeric structures solving the linearized Poisson-Boltzmann equation using the APBS software,[24] and the binding energy in vacuo using the Amber force field.[25] Protein dimers were extrapolated from the X-ray structure of α-TTP_S (PDB:5MUE).[11]

The four IS are identified by four vectors with origin in the center of the hard sphere, and ends

in:

$$\begin{aligned} \mathrm{IS_A} &= (0, R, 0) \\ \mathrm{IS_B} &= (-R, 0, 0) \\ \mathrm{IS_C} &= \left(0, \frac{R}{\sqrt{2}}, -\frac{R}{\sqrt{2}}\right) \\ \mathrm{IS_D} &= \left(\frac{R}{\sqrt{2}}, 0, -\frac{R}{\sqrt{2}}\right) \end{aligned} \tag{1}$$

where R = 2 nm is the radius of a hard sphere with its center in $O(0, 0, 0)$.

The potential energies between the $\mathrm{IS_A}$-$\mathrm{IS_B}$ and $\mathrm{IS_C}$-$\mathrm{IS_D}$ couples are described by the following well potentials:

$$E_{\mathrm{A/B}}(r, \psi, \phi) = \begin{cases} 0 & r > r_{cut} \\ E_{\mathrm{A/B}} \cos\psi \cos\phi & r \leqslant r_{cut} \end{cases} \tag{2}$$

$$E_{\mathrm{C/D}}(r, \psi, \theta) = \begin{cases} 0 & r > r_{cut} \\ E_{\mathrm{C/D}} \cos\psi \cos 2\theta & r \leqslant r_{cut} \end{cases} \tag{3}$$

where r is the IS-IS distance, $r_{cut} = 0.2\,R$ is the maximum range of the interaction. $\cos\psi, \cos\phi, \cos\theta$ are defined from the scalar multiplication of the normalized vectors as in figure 2. The angular dependency is necessary to model both the chirality of the protein, and that protein binding occurs over an extended surface that requires a well-defined orientation of the two partners.

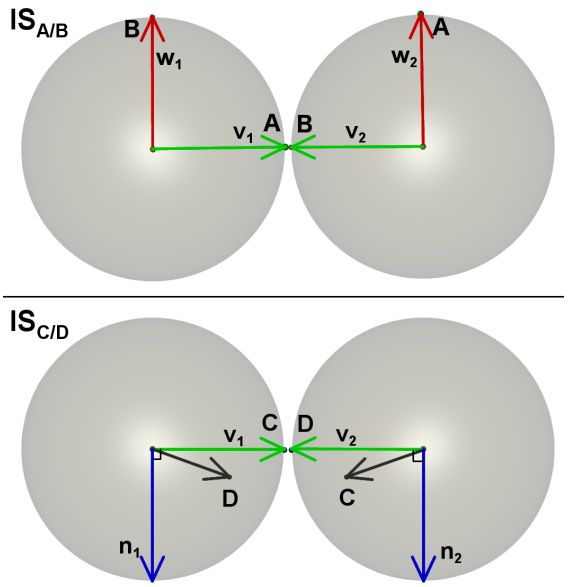

Figure 2: Normalized vectors used to define the angular dependency of the interaction energy. $\cos\psi = \mathbf{v_1} \cdot \mathbf{v_2}$, for any A/B or C/D interaction (green arrows); $\cos\phi = \mathbf{w_1} \cdot \mathbf{w_2}$ for any A/B interaction (top panel, red arrows); $\cos\theta = \mathbf{n_1} \cdot \mathbf{n_2}$, for any C/D interaction (bottom panel, blue arrows)

System setup We simulated a system having N = 216 particles at thermal equilibrium. The protein particles were initially distributed uniformly in a periodic cubic simulation box of edge 24.625 R (where R is the radius of the protein), corresponding to roughly the experimental concentration at which α-TTP aggregation is observed.[11] The accessible conformational space in the canonical NVT ensemble was explored using a Metropolis Monte Carlo (MC) algorithm.[26]

Random moves included the rotation or translation of the single particles or whole clusters of bound particles.[27–29] A bond between two particles was assumed to exist if the distance between the corresponding interaction sites was less than 0.2 R. Two particles were considered to belong to same cluster if they were connected by a chain of bonds.[30] Rotational moves made use of quaternion representation of the particle's orientation, which was modified by a smaller random orientation and then renormalized.[27,28]

The canonical ensemble was sampled at different values of the temperature, in order to determine thermodynamic regimes at which different α-TTP aggregates exist. All the simulations at different temperatures started from a random configuration of the proteins in the box. Simulations

were organized in cycles, each cycle consisting of a number of attempted particle moves. Typical equilibration runs consisted of 6 $\times 10^6$ - 9 $\times 10^6$ MC cycles and were followed by a production run of additional 3×10^5 MC cycles, during which averages of energy and cluster abundance were calculated. Convergence of the results was tested by evaluating both the convergence of the expectation value of the energy, and comparing the variance to the typical short time (1000 steps) energy fluctuations at a given temperature over the last 6×10^5 MC cycles.

The acceptance probability for the single particle moves like translation or rotation was evaluated according to:

$$\left\{ \begin{array}{ll} \text{if } E_t \leqslant E_i, & P(acc) = 1 \\ \text{if } E_t > E_i, & P(acc) = \exp(-\beta(E_t - E_i)) \end{array} \right\} \tag{4}$$

Here P is the acceptance probability, E_i the initial Energy and E_t the energy after the test step. β is the reciprocal thermodynamic temperature of the system. The cluster moves were implemented following the early rejection scheme.[27]

All results here are presented in reduced units: $\mathbf{U}^* = U/u$ and $\mathbf{T}^* = k_B T/u$ for the inner energy and the temperature of the system.

Trajectory analysis was performed using the tools available in the VMD 1.9.2 package.[31]

Results and Discussion

In a first set of MC runs, we investigated the existence of α-TTP aggregates when only the $\mathrm{IS_{A/B}}$ interface is active. This setup mimics the experimental conditions at which the N-terminal region is folded, and the $\mathrm{IS}_{C/D}$ is not exposed to the solvent. The top panel of figure 3 shows the relative abundance of α-TTP aggregates as a function of the thermal energy. At high temperatures, only monomeric species are present. At around $\mathbf{T}^*$ u = 0.09 E_{AB}, we observed the appearance of low weight aggregates, mostly tetramers, with also a non-negligible presence of trimers and dimers. Lowering the temperature stabilises the tetrameric packing, which corresponds to the aggregation state of four α-TTP proteins around the C_4 Symmetry axis in α-TTP_S (Figure S1). Higher molec-

ular weight structures, for example, linear chain-like structures along sequences of $IS_{A/B}$ contacts were not observed, as they are forbidden by the chirality condition on the interaction energy, which only allows the formation of ring-like tetramers.

In a second set of MC simulations, both the $IS_{A/B}$, $IS_{C/D}$ interactions were active. This setup mimics α-TTP with an unfolded N-terminus. In this case, we observed three temperature regimes at which distinct aggregation states appear (Figure 3 (Bottom)). In the high temperature range ($\mathbf{T}^* > 0.25$), only α-TTP monomers were present. In the narrow ($0.10 < \mathbf{T}^* < 0.25$) region, we detected the formation of trimeric species (α-TTP_3), while for ($\mathbf{T}^* < 0.12$) the systems rapidly evolved in high-weight aggregates (α-TTP_S) (Figure 6).

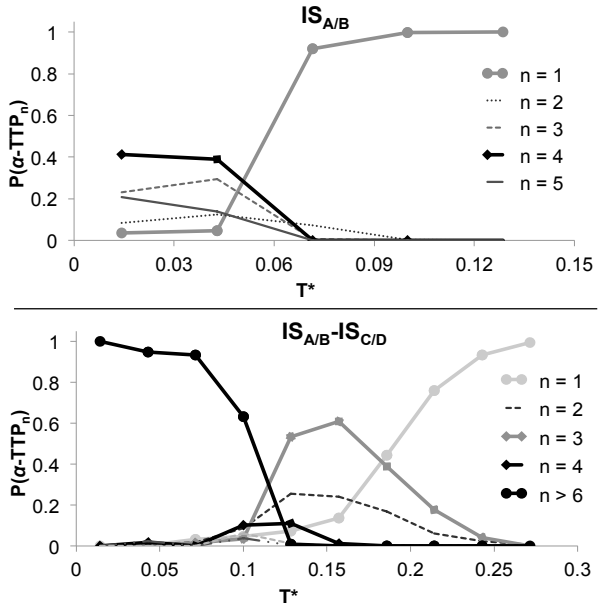

Figure 3: Aggregation states of α-TTP (α-TTP_n) as a function of the reduced temperature $\mathbf{T}^*$, (*top panel*) when only the $IS_{A/B}$ interface is active, or (*bottom panel*) when both the $IS_{A/B}$ and $IS_{C/D}$ interfaces are active.

The trimeric phase includes aggregates built along the $IS_{C/D}$ interface. In fact, α-TTP_3s are stable in a temperature range at which the thermal energy is too high to allow the formation of A/B contacts. The structure of α-TTP_3 corresponds to the assembly of three α-TTP proteins around the C_3 axis of α-TTP_S. The high-weight aggregates appearing for ($T^* < 0.12$) are constituted by oligomerization of α-TTP_3, up to α-TTP_S by formation of $IS_{A/B}$ contacts.

During the MC runs, we observed a marginal degree of poly-dispersion especially near the transition temperatures (Figure 3). Nonetheless, the profile of the energy as a function of the temperature shows two clear sigmoidal jumps, indicating the presence of two distinct first-order phase transitions from α-TTP to α-TTP$_3$, to α-TTP$_S$ (Figure 4).

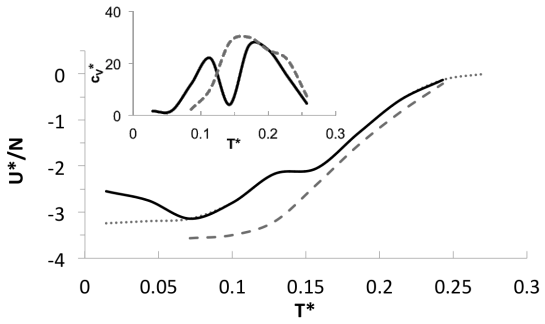

Figure 4: Inner energy per protein $\mathbf{U^*/N}$, and specific heat $\mathbf{c}_{\mathrm{V}}^*$ (inset) as a function of the reduced temperature for the system with both active IS$_{\mathrm{A/B}}$ and IS$_{\mathrm{C/D}}$ (continuous line). The dotted line was obtained by simulated annealing starting from converged data at T*=0.07. The dashed lines report the same data for the system with E$_{A/B}$= 1.5 u.

Oligomerization to α-TTP$_S$ begins at a higher temperature ($\mathbf{T}^* = 0.12$) than the one characterizing α-TTP aggregation when only IS$_{A/B}$ are active ($\mathbf{T}^* = 0.07$). In fact, α-TTP$_3$ dimerization involves binding over two IS$_{A/B}$ contacts, producing a hexameric structure centered around a C_2 symmetry axis corresponding to one of the C_2 axes of α-TTP$_S$. Simultaneous formation of two IS$_{A/B}$ interactions is facilitated by the pre-organization of the interaction sites along the edges of the rigid α-TTP$_3$.

The cooperative effect of the IS$_{A/B}$ onto the binding of α-TTP$_3$ is responsible for the absence of intermediate weight aggregates between α-TTP$_3$ and α-TTP$_S$. Practically, the assembly of α-TTP$_S$ may be schematically seen as the progressive dimerization of α-TTP$_3$, α-TTP$_6$, and α-TTP$_{12}$ over two, four, and eight IS$_{A/B}$ contacts (Figure 5). Below the critical temperature that allows the first dimerization of α-TTP$_3$, further assemblies involve increasingly larger numer of IS$_{A/B}$ interactions, yielding α-TTP$_S$.

The existence of a region of thermodynamic stability for α-TTP$_3$ depends on the relative magnitude of E$_{A/B}$ versus E$_{C/D}$. To verify that, we ran one additional set of MC simulations on a

system where $\mathrm{E}_{A/B} = 1.5\ u$. In this case, we expected the critical temperature for the formation of α-TTP$_3$ to be very similar to that of α-TTP$_3$ dimerization. In fact, we observed only one sigmoidal profile of the $\mathbf{U}^*$ vs. $\mathbf{T}^*$ plot, indicating the coalescence of the two phase transitions into one (Figure 4), and a direct aggregation from α-TTP to α-TTP$_S$.

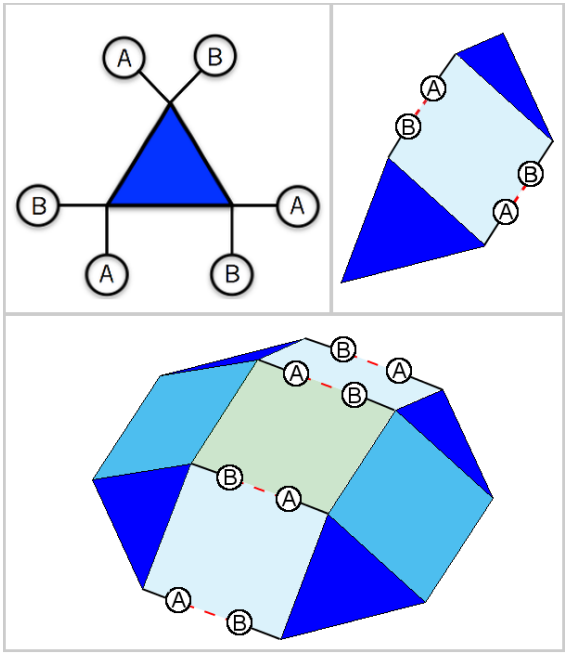

Figure 5: Oligomerization of α-TTP$_3$ (Blue triangle). Each oligomerization step involves the formation of at least two IS$_{A/B}$ contacts. Newly formed contacts are represented by dashed lines.

Although our MC runs depict the clear tendency of the system to form α-TTP$_S$, statistically, we obtained the formation of imperfect spherical complexes with an average aggregation number of 20.2. The presence of defects is visible from the average energy per protein reported in Figure 4, which is always larger than the ideal value of -4u even for low values of the thermal energy. The formation of defectuous α-TTP$_S$ assemblies is due convergence issues related to the appearance of kinetically trapped states at lower temperatures. These states are dominant in MC runs at values of $\mathbf{T}^* u \ll \mathrm{E}_{\mathrm{A/B}}$, which yielded poorly aggregated structures, with energies consistently higher than the best organized α-TTP$_S$-like structures found at higher values of the temperature. Improvement of the sampled structures at $\mathbf{T}^* \leqslant 0.06$ was obtained by applying 30 cycles of simulated annealing, between $\mathbf{T}^* = 0.07$ and the target temperature. In this case, we could observe the formation more

regular α-TTP$_S$ structures with aggregation number ≈ 23.

Overall, our data are in optimal agreement with the native gel electrophoresis experiment reported in ref.[11] In particular, natively folded α-TTP, which can oligomerize only through the A/B interface, showed the predominance of a monomeric form, with residual presence of low-weight aggregates (dimer, tetramer, figure 3). On the contrary, after triggering aggregation by unfolding of the N-terminus, the proteins assembled into stable α-TTP$_S$, which showed no tendency to disgregate back into lighter oligomers in further incubation tests over a time-window of 24 hours.[11] Thus, the experimental condition of the real system would correspond to the region of $\mathbf{T}^* \approx$ 0.06-0.08 in our toy system, where the folded state is mostly monomeric, while the partially unfolded state yields almost pure α-TTP$_S$ (figure 6).

Apart from α-TTP and α-TTP$_S$, α-TTP$_3$ is another oligomerization state for which, when IS$_{C/D}$ is active, there exists a region of thermodynamical stability. The nature of α-TTP$_3$ as a true thermodynamic stable aggregate is confirmed by a diverging specific heat in correspondence of the boundary transition temperatures $\mathbf{T}^* \approx$ 0.11, 0.18 (figure 4, inset), which is a clear indication of the presence of two separate phase transitions. Experimentally, native α-TTP rapidly evolves into α-TTP$_S$, indicating that ambient thermodynamic conditions fall in the region of stability of the phase diagram for α-TTP$_S$, nonetheless α-TTP$_3$ should be the dominating species in an intermediate region at higher temperature. The narrowness of such a region depends on the relative strength of IS$_{A/B}$ and IS$_{C/D}$.

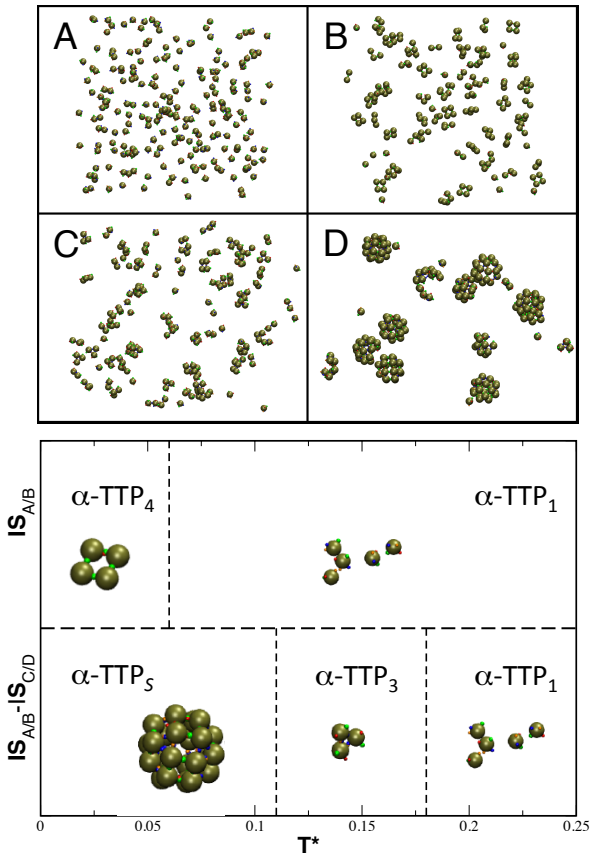

Figure 6: *Top*: Aggregation states of α-TTP at different conditions. *Panel A:* monomeric dispersion at $\mathbf{T}^*$ = 0.27; *Panel B:* aggregation of low-weight oligomers at $\mathbf{T}^*$= 0.04, for the system with only active $\mathrm{IS_{A/B}}$; *Panel C:* system with all active IS's at intermediate $\mathbf{T}^*$ = 0.13, where trimers begin to form; *Panel D:* same system at $\mathbf{T}^*$ = 0.07, characterized by formation of α-TTP_S. *Bottom:* Phase diagram with dominating species at different conditions of temperature and folded state. The region between 0.06 and 0.11 $\mathbf{T}^*$ corresponds to the experimentally observed behavior, with either properly folded monomers, or assembled α-TTP_S.

According to our results, point mutations at the surface of the protein that either weaken the $\mathrm{IS}_{A/B}$ interaction or, alternatively, strengthen the $\mathrm{IS}_{C/D}$ interaction would both yield to an enlargement of the region of stability for α-TTP_3. In our previous study, the analysis of the α-TTP_S protein-protein interfaces at the four-fold symmetry revealed hydrophobic contact areas that are mostly responsible for binding (figure 7).[11] Introducing specific point-mutations of these key residues can have stark impact on particle assembly. Any disruptive mutation like, for example F165R, where a positively charged residue is introduced into the hydrophobic patch through site-directed mutagenesis, should weaken the cooperative effects of the $\mathrm{IS}_{A/B}$. In this way, it should be

possible to inactivate progressive dimerization, favoring instead α-TTP$_3$ as the dominating species.

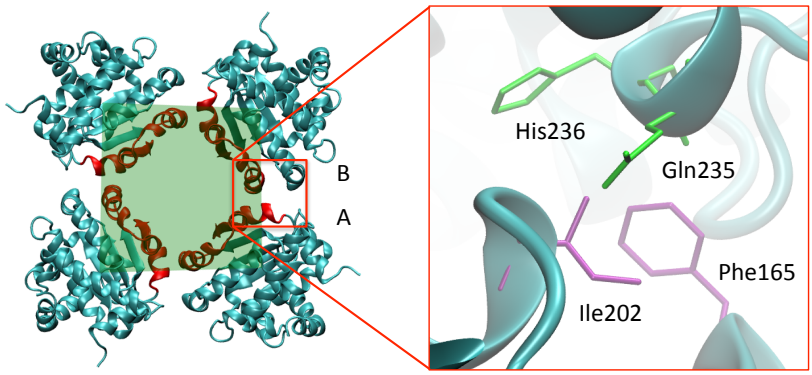

Figure 7: α-TTP interaction at the *Left:* Structure of the assembly of α-TTParound the C_4 symmetry axis of α-TTP$_S$. The structure interlocked via multiple IS$_{AB}$, topologically located at the ligand binding site region of α-TTP. *Right:* the most relevant residues responsible for the binding at this interface are shown in licorice. The green and purple colors refer to amino acids belonging to two different α-TTP units.

Interestingly, partial α-TTP aggregation is not strictly bound to the unfolding of the N-terminus. Rather, low-weight aggregates of folded α-TTP can be formed by binding through the natively solvent-exposed A/B interface. The transition from monomers to A/B dimers or tetramers is determined by the balance between the A/B binding energy and the dimerization entropy loss. In solution, this balance is in favor of the monomeric species. Nonetheless, external factors like pre-organization of the monomers on a surface, may favor the formation of such oligomers. Data by Arai and co-workers[3] reported that a mixture of α-TTP, α-tol, and lipid fractions containing different PIPs such such as PI(3,4)P2 or PI(4,5)P2 induced the formation of α-TTP tetramers. In this study, also crystals of such ternary mixtures were analyzed by x-ray crystallography at 2.6 or 2.0 Å resolution, respectively. Superposition of the open (PDB: 1OIZ), closed (PDB: 1OIP), and PI(4,5)P2-bound (PDB: 3W68) structures revealed a semi opened mobile gate conformation in the ternary structure of α-TTP.[3] It was also shown that such ternary complexes possess inter-membrane transfer activity *in vitro* when using donor or acceptor liposomes doped with PIPs. Neither α-TTP$_3$ nor α-TTP$_S$ aggregates were reported in this study. This is in accordance with our previous observations that aggregation into spherical particles occur only when α-tol is bound to α-TTP with the mobile gate being in its fully closed state, and subsequent unfolding of the N-terminus has

unmasked the trimeric interaction interface of α-TTP.

Concluding remarks

Our model provides a description of the thermodynamically stable aggregation states of α-TTP that is consistent with experimental data. We report the existence of a metastable low-weight oligomerization state (α-TTP$_3$) that is key to the fast and regular assembly of α-TTP$_S$.

Expression of functional mutants with different assembling properties should be feasible by minimal modifications of the native sequence. Studies by Kortemme et al.[32] have shown in other systems that in general a single mutation is sufficient to redesign functional protein-protein interfaces and thus alter specificity. Interestingly, self-assembly into a similar spherical homo-multimer structure composed by 24 monomers has been reported in ferritin, an evolutionarily unrelated protein than α-TTP.[33] In a very recent study, Dmochowsky and coworkers showed that that a homo dimeric state represents a common intermediate during protein cage assembly of the 24-meric ferritin, and that the dimer/24mer balance can be experimentally altered by introducing single positive charges at sites along the dimer-dimer interface.[34] It is important to notice that even small variations in the binding affinity can have a very large impact in the assembling process, due to the cooperativity effects taking place during the assembling, as evidenced in the present study.

Functional low-weight oligomers such as α-TTP$_3$ may play a crucial role for transcytosis through endothelial membranes. Our former transfection studies[11] showed that the transcytotic flux does not follow a diffusive regime, with larger α-TTP$_S$ transfecting at a faster rate than smaller monomeric α-TTP. In fact, the delay observed in the α-TTP flux may imply that aggregation of a minimal unit larger than the monomer is required to the activate the transport. Further studies introducing disruptive mutations at the trimeric or tetrameric interfaces could help the understanding of the assembly kinetics and thermodynamics at different physiological conditions. Most importantly, they may lead to the identification of the minimal biologically active units that are active for the transfection through the endothelium, a crucial step toward the engineering of these protein for

targeted drug delivery.

Associated Content

The authors declare no competing financial interest.

Acknowledgement

This work was supported by the Research Council of Norway (RCN) through the CoE Hylleraas Centre for Quantum Molecular Sciences Grant No. 262695, and by the Norwegian Supercomputing Program (NOTUR) (Grant No. NN4654K). HBK received funding from the European Union Horizon 2020 research and innovation programme under the Marie Skłodowska-Curie grant agreement No. 704491.

References

(1) Traber, M. G.; Sokol, R. J.; Burton, G. W.; Ingold, K. U.; Papas, A. M.; Huffaker, J. E.; Kayden, H. J. Impaired ability of patients with familial isolated vitamin E deficiency to incorporate α-tocopherol into lipoproteins secreted by the liver. *J. Clin. Invest.* **1990**, *85*, 397–407.

(2) Traber, M. G.; Burton, G. W.; Hamilton, R. L. Vitamin E trafficking. *Ann. N. Y. Acad. Sci.* **2004**, *1031*, 1–12.

(3) Kono, N.; Ohto, U.; Hiramatsu, T.; Urabe, M.; Uchida, Y.; Satow, Y.; Arai, H. Impaired α-TTP-PIPs interaction underlies familial vitamin E deficiency. *Science* **2013**, *340*, 1106–1110.

(4) Meier, R.; Tomizaki, T.; Schulze-Briese, C.; Baumann, U.; Stocker, A. The molecular basis of vitamin E retention: Structure of human α-tocopherol transfer protein. *J. Mol. Biol.* **2003**, *331*, 725–734.

(5) Min, K. C.; Kovall, R. a.; Hendrickson, W. a. Crystal structure of human alpha-tocopherol transfer protein bound to its ligand: implications for ataxia with vitamin E deficiency. *Proc. Natl. Acad. Sci. U. S. A.* **2003**, *100*, 14713–14718.

(6) Sha, B.; Phillips, S. E.; Bankaitis, V. A.; Luo, M. Crystal structure of the Saccharomyces cerevisiae phosphatidylinositol-transfer protein. *Nature* **1998**, *391*, 506–510.

(7) Stocker, A.; Tomizaki, T.; Schulze-Briese, C.; Baumann, U. Crystal structure of the human supernatant protein factor. *Structure* **2002**, *10*, 1533–1540.

(8) He, X.; Lobsiger, J.; Stocker, A. Bothnia dystrophy is caused by domino-like rearrangements in cellular retinaldehyde-binding protein mutant R234W. *Proc. Natl. Acad. Sci. U. S. A.* **2009**, *106*, 18545–18550.

(9) Stocker, A. Molecular mechanisms of vitamin E transport. *Ann. N. Y. Acad. Sci.* **2004**, *1031*, 44–59.

(10) Chung, S.; Ghelfi, M.; Atkinson, J.; Parker, R.; Qian, J.; Carlin, C.; Manor, D. Vitamin E and phosphoinositides regulate the intracellular localization of the hepatic α-tocopherol transfer protein. *J. Biol. Chem.* **2016**, *291*, 17028–17039.

(11) Aeschimann, W.; Staats, S.; Kammer, S.; Olieric, N.; Jeckelmann, J. M.; Fotiadis, D.; Netscher, T.; Rimbach, G.; Cascella, M.; Stocker, A. Self-assembled α-Tocopherol Transfer Protein Nanoparticles Promote Vitamin E Delivery Across an Endothelial Barrier. *Sci. Rep.* **2017**, *7*, 1–13.

(12) Saraiva, C.; Praça, C.; Ferreira, R.; Santos, T.; Ferreira, L.; Bernardino, L. Nanoparticle-mediated brain drug delivery: Overcoming blood-brain barrier to treat neurodegenerative diseases. *J. Control. Release* **2016**, *235*, 34–47.

(13) Deli, M. A.; Ábrahám, C. S.; Kataoka, Y.; Niwa, M. Permeability studies on in vitro blood-

brain barrier models: Physiology, pathology, and pharmacology. *Cell. Mol. Neurobiol.* **2005**, *25*, 59–127.

(14) Zhang, Z.; Glotzer, S. C. Self-assembly of patchy particles. *Nano Lett.* **2004**, *4*, 1407–1413.

(15) Sciortino, F.; Giacometti, A.; Pastore, G. Phase Diagram of Janus Particles. *Phys. Rev. Lett.* **2009**, *103*, 237801.

(16) Kraft, D. J.; Ni, R.; Smallenburg, F.; Hermes, M.; Yoon, K.; Weitz, D. A.; van Blaaderen, A.; Groenewold, J.; Dijkstra, M.; Kegel, W. K. Surface roughness directed self-assembly of patchy particles into colloidal micelles. *Proc. Natl. Acad. Sci. U.S.A.* **2012**, *109*, 10787–10792.

(17) Wilber, A. W.; Doye, J. P. K.; Louis, A. A.; Noya, E. G.; Miller, M. A.; Wong, P. Reversible self-assembly of patchy particles into monodisperse icosahedral clusters. *J. Chem. Phys.* **2007**, *127*, 085106.

(18) Carlsson, F.; Linse, P.; Malmsten, M. Monte Carlo simulations of polyelectrolyte-protein complexation. *J. Phys. Chem. B* **2001**, *105*, 9040–9049.

(19) Fantoni, R.; Gazzillo, D.; Giacometti, A.; Miller, M. A.; Pastore, G. Patchy sticky hard spheres: Analytical study and Monte Carlo simulations. *J. Chem. Phys.* **2007**, *127*, 234507.

(20) Villar, G.; Wilber, A. W.; Williamson, A. J.; Thiara, P.; Doye, J. P.; Louis, A. A.; Jochum, M. N.; Lewis, A. C.; Levy, E. D. Self-assembly and evolution of homomeric protein complexes. *Phys. Rev. Lett.* **2009**, *102*, 118106.

(21) Liu, H.; Kumar, S. K.; Douglas, J. F. Self-Assembly-Induced Protein Crystallization. *Phys. Rev. Lett.* **2009**, *103*, 018101.

(22) Li, Y.; Shi, T.; An, L.; Huang, Q. Monte Carlo Simulation on Complex Formation of Proteins and Polysaccharides. *J. Phys. Chem. B* **2012**, *116*, 3045–3053.

(23) Li, W.; Persson, B. A.; Morin, M.; Behrens, M. A.; Lund, M.; Zackrisson Oskolkova, M. Charge-induced patchy attractions between proteins. *J. Phys. Chem. B* **2015**, *119*, 503–508.

(24) Baker, N. A.; Sept, D.; Joseph, S.; Holst, M. J.; McCammon, J. A. Electrostatics of nanosystems: Application to microtubules and the ribosome. *Proc. Natl. Acad. Sci. U.S.A.* **2001**, *98*, 10037–10041.

(25) Hornak, V.; Abel, R.; Okur, A.; Strockbine, B.; Roitberg, A.; Simmerling, C.; Brook, S.; Brook, S.; Brook, S. Comparison of multiple AMBER force fields and development of improved protien backbone parameters. *Proteins* **2006**, *65*, 712–725.

(26) Metropolis, N.; Rosenbluth, A. W.; Rosenbluth, M. N.; Teller, A. H.; Teller, E. Equation of state calculations by fast computing machines. *J. Chem. Phys.* **1953**, *21*, 1087–1092.

(27) Frenkel, D.; Smit, B. *Understanding Molecular Simulation*, 2nd ed.; Academic Press, Inc.: Orlando, FL, USA, 2001.

(28) Allen, M. P.; Tildesley, D. J. *Computer Simulation of Liquids*; Clarendon Press: New York, NY, USA, 1987.

(29) Wu, D.; Chandler, D.; Smit, B. Electrostatic analogy for surfactant assemblies. *J. Phys. Chem.* **1992**, *96*, 4077–4083.

(30) Miller, M. A.; Amon, L. M.; Reinhardt, W. P. Should one adjust the maximum step size in a Metropolis Monte Carlo simulation? *Chem. Phys. Lett.* **2000**, *331*, 278–284.

(31) Humphrey, W.; Dalke, A.; Schulten, K. VMD: Visual molecular dynamics. *J. Mol. Graph.* **1996**, *14*, 33–38.

(32) Kortemme, T.; Joachimiak, L. A.; Bullock, A. N.; Schuler, A. D.; Stoddard, B. L.; Baker, D. Computational redesign of protein-protein interaction specificity. *Nat. Struct. Mol. Biol.* **2004**, *11*, 371–379.

(33) Lawson, D. M.; Artymiuk, P. J.; Yewdall, S. J.; Smith, J. M. A.; Livingstone, J. C.; Treffry, A.; Luzzago, A.; Levi, S.; Arosio, P.; Cesareni, G.; Thomas, C. D.; Shaw, W. V.; Harrison, P. M. Solving the structure of human H ferritin by genetically engineering intermolecular crystal contacts. *Nature* **1991**, *349*, 541–544.

(34) Pulsipher, K. W.; Villegas, J. A.; Roose, B. W.; Hicks, T. L.; Yoon, J.; Saven, J. G.; Dmochowski, I. J. Thermophilic ferritin 24mer assembly and nanoparticle encapsulation modulated by interdimer electrostatic repulsion. *Biochemistry* **2017**, *56*, 3596–3606.

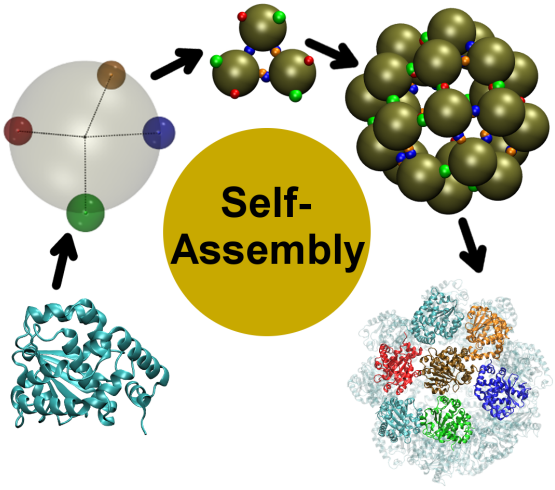

Table of Contents